JACS
JOURNAL OF THE AMERICAN CHEMICAL SOCIETY

Article

pubs.acs.org/JACS

Dye Molecular Structure Device Open-Circuit Voltage Correlation in Ru(II) Sensitizers with Heteroleptic Tridentate Chelates for Dye-Sensitized Solar Cells

Kuan-Lin Wu,[†,⊥] Cheng-Hsuan Li,[†,⊥] Yun Chi,*[,†] John N. Clifford,[‡] Lydia Cabau,[‡] Emilio Palomares,*[,‡,§] Yi-Ming Cheng,[∥] Hsiao-An Pan,[∥] and Pi-Tai Chou*[,∥]

[†]Department of Chemistry and Low Carbon Energy Research Center, National Tsing Hua University, Hsinchu 30013, Taiwan

[‡]Institute of Chemical Research of Catalonia (ICIQ), Avda. Països Catalans 16, 43007 Tarragona, Spain

[§]ICREA, Avda. Lluís Companys 28, Barcelona E-08030, Spain

[∥]Department of Chemistry and Center for Emerging Material and Advanced Devices, National Taiwan University, Taipei 10617, Taiwan

Supporting Information

ABSTRACT: Dicarboxyterpyridine chelates with π-conjugated pendant groups attached at the 5- or 6-position of the terminal pyridyl unit were synthesized. Together with 2,6-bis(5-pyrazolyl)pyridine, these were used successfully to prepare a series of novel heteroleptic, bis-tridentate Ru(II) sensitizers, denoted as **TF-11**−**14**. These dyes show excellent performance in dye-sensitized solar cells (DSCs) under AM1.5G simulated sunlight at a light intensity of 100 mW cm^{-2} in comparison with a reference device containing $[Ru(Htctpy)(NCS)_3][TBA]_3$ (**N749**), where H_3tctpy and TBA are 4,4′,4″-tricarboxy-2,2′:6′,2″-terpyridine and tetra-*n*-butylammonium cation, respectively. In particular, the sensitizer **TF-12** gave a short-circuit photocurrent of 19.0 mA cm^{-2}, an open-circuit voltage (V_{OC}) of 0.71 V, and a fill factor of 0.68, affording an overall conversion efficiency of 9.21%. The increased conjugation conferred to the TF dyes by the addition of the π-conjugated pendant groups increases both their light-harvesting and photovoltaic energy conversion capability in comparison with **N749**. Detailed recombination processes in these devices were probed by various spectroscopic and dynamics measurements, and a clear correlation between the device V_{OC} and the cell electron lifetime was established. In agreement with several other recent studies, the results demonstrate that high efficiencies can also be achieved with Ru(II) sensitizers that do not contain thiocyanate ancillaries. This bis-tridentate, dual-carboxy anchor configuration thus serves as a prototype for future omnibearing design of highly efficient Ru(II) sensitizers suited for use in DSCs.

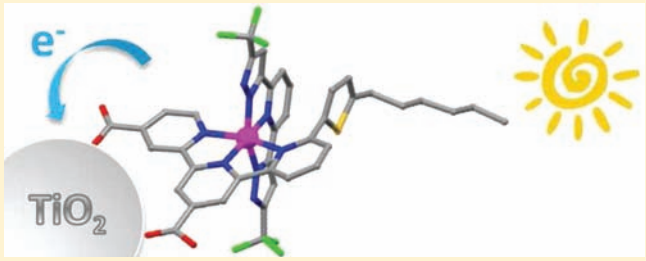

Dye-sensitized solar cells (DSCs) have received significant attention as potential low-cost alternatives to conventional semiconductor-based solar cells made from silicon.[1−7] In a DSC, a suitable sensitizer/dye is deposited on a porous film made of a nanocrystalline metal oxide such as TiO_2. Upon illumination with solar radiation, the photoinjected electrons diffuse through the interconnected mesoporous particles and are then extracted at the anode, while the oxidized sensitizer is rapidly regenerated by the I^-/I_3^- redox couple in the electrolyte solution. The oxidized I_3^- diffuses to the cathode and is reduced back to I^- to complete the regenerative process.[8,9]

Among the fruitful progress made for DSCs, the innovative design of the dye sensitizer is of pivotal importance in achieving high efficiency. Typical sensitizers include both pure organic (i.e., metal-free) and organometallic (i.e., metal-containing) dyes,[10−13] for which the Ru(II)-based sensitizers are superior to most others and are capable of producing certified cells with impressive efficiencies of up to ∼11.7%.[14] The most studied Ru(II) dyes, which may be considered as the templates for this class of dye, are known as $[Ru(H_2dcbpy)_2(NCS)_2]$ (**N3**) and $[Ru(Hdcbpy)_2(NCS)_2][TBA]_2$ (**N719**), where H_2dcbpy and TBA are 4,4′-dicarboxy-2,2′-bipyridine and tetra-*n*-butylammonium cation, respectively. Another much studied dye is the panchromatic sensitizer $[Ru(Htctpy)(NCS)_3][TBA]_3$ (**N749**), where H_3tctpy is 4,4′,4″-tricarboxy-2,2′:6′,2″-terpyridine. This dye is notable for its ability to harvest solar radiation extending into the near-IR region.[15] Importantly, all of these Ru(II) sensitizers possess thiocyanate ancillaries, whose intimate involvement in the regeneration process with the I^-/I_3^- redox couple has been confirmed experimentally and also using DFT calculations.

A significant departure from the above molecular design was recently reported by van Koten and co-workers,[16,17] who demonstrated that cyclometalating chelates are capable of

Received: January 25, 2012
Published: April 16, 2012

ACS Publications © 2012 American Chemical Society

dx.doi.org/10.1021/ja300828f | J. Am. Chem. Soc. 2012, 134, 7488−7496

preserving the light-harvesting properties of a class of bis-tridentate Ru(II) complexes. Subsequently, Grätzel and co-workers announced the design of tris-bidentate $[Ru(H_2dcbpy)_2(dfppy)]^+$, where dfppy is 4,6-difluorophenylpyridinato, which in the absence of thiocyanate can still afford a high conversion efficiency (η) of 10.1%, suggesting that the almost ever present thiocyanate is not a complete necessity in the design of efficient Ru(II) sensitizers.[18] Subsequent studies demonstrating the advantages of using cyclometalating chelates in the assembly of thiocyanate-free Ru(II) complexes for DSC applications were independently reported by Berlinguette and co-workers.[19,20] A high η of 8.02% has been documented for both tricarboxyterpyridine and dicarboxybipyridine Ru(II) complexes that are devoid of thiocyanate ligands.[21]

Complementary to the aforementioned progress, our research team has been involved in the functionalization of Ru(II) sensitizers with either bidentate or tridentate azolate chelates.[22−25] It is believed that the azolic group may be more reactive than the traditional heterocyclic cyclometalates because of the greater N−H acidity. Moreover, the stronger electron-withdrawing character of azolate is also capable of increasing the oxidation potential of Ru(II) sensitizers containing these ligands, which is essential for the facile regeneration of the oxidized sensitizers by the I^-/I_3^- redox couple. Indeed, only with cyclometalate chelates possessing sufficient electron-deficient character has it been possible to achieve satisfactorily high η under typical device operation conditions.[19]

In yet another approach, we recently reported a class of tricarboxyterpyridine Ru(II) complexes such as **TF-1** and **TF-2** (Scheme 1), which contain as ancillary ligands 2,6-bis(3-trifluoromethylpyrazol-5-yl)pyridine and its derivative bearing a π-conjugated pendant group, respectively.[26] These sensitizers allow for excellent DSCs with η values of up to 10.7%. Moreover, we also speculated that the π-conjugated pendant group at the ancillary site could alternatively be placed on the terpyridine ligand, rendering sensitizers showing comparable or perhaps even better efficiencies in DSC devices. The desired dicarboxyterpyridine chelates and the associated Ru(II) complexes such as **PRT-11** and **PRT-12** (Scheme 1) were successfully synthesized in our previous approach.[27] Efforts have thus switched to combining both the dicarboxyterpyridine and dianionic 2,6-bis(3-trifluoromethylpyrazol-5-yl)pyridine ancillary ligands in the assembly of a new class of bis-tridentate Ru(II) sensitizers that contain no thiocyanate ligands. In this study, we report the synthesis and structural and spectroscopic characterization of four such novel Ru(II) complexes as well as their performance and properties in DSCs. The prospects for these novel dye sensitizers to serve as sensitizers in stable, high-efficiency DSCs is moreover discussed.

Scheme 1. Structures of the Ru(II) Sensitizers TF-1, TF-2, PRT-11, and PRT-12

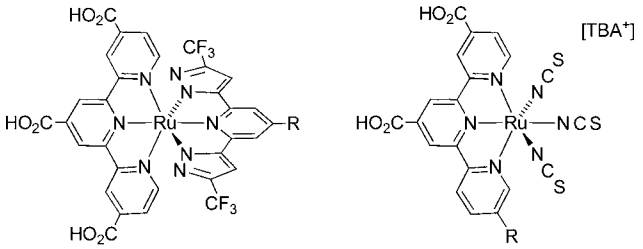

TF-1, R = H
TF-2, R = 5-(2-hexylthiophene)
PRT-11, R = H
PRT-12, R = 5-(2-hexylthiophene)

EXPERIMENTAL SECTION

General Procedures. All of the reactions were performed under an argon atmosphere, and solvents were distilled from appropriate drying agents prior to use. Commercially available reagents were used without further purification, unless otherwise stated. All reactions were monitored using precoated thin-layer chromatography plates (0.20 mm with fluorescent indicator UV254). Mass spectra were obtained on a JEOL SX-102A instrument operated in either electron impact (EI) or fast atom bombardment (FAB) mode. ^{1}H and ^{13}C NMR spectra were recorded on a Varian Mercury-400 or INOVA-500 instrument. Elemental analysis was carried out with a Heraeus CHN-O Rapid Elementary Analyzer.

Synthesis of TF-11. Ligand **L1** (375 mg, 0.69 mmol) and $RuCl_3{\cdot}3H_2O$ (198 mg, 0.76 mmol) in 15 mL of absolute ethanol was refluxed for 4 h. The mixture was cooled to room temperature (RT) and filtered. The precipitate was washed with ethanol and dried in vacuum to give a brown solid. This brown solid (100 mg, 0.133 mmol) was then mixed with 2,6-bis(3-trifluoromethyl-1*H*-pyrazol-5-yl)-pyridine (45.4 mg, 0.133 mmol) and KOAc (65.3 mg, 0.67 mmol) in 15 mL of toluene and refluxed for 6 h. After cooling to RT, the solvent was removed by rotary evaporation. The residue was dissolved in CH_2Cl_2, washed with water, and dried over anhydrous $MgSO_4$. After removal of the solvent, the residue was purified by silica gel column chromatography, eluting with ethyl acetate. The obtained brown solid was then dissolved in a mixture of 10 mL of acetone and 0.57 mL of 0.5 N NaOH. The resulting solution was brought to reflux for 3 h and then cooled to RT and concentrated. The residue was dissolved in excess water and titrated with 2 N HCl solution to reach pH 3. The precipitate was collected and washed with water, CH_2Cl_2, and acetone in sequence to yield the pure product **TF-11** (42.9 mg, 33%).

Selected Spectral Data for ***TF-11****.* MS (FAB, ^{102}Ru): m/z 935 [M + H]$^+$. ^{1}H NMR (500 MHz, DMSO-d_6, 298 K): δ 9.30 (s, 1H), 9.18 (s, 1H), 9.11 (s, 1H), 8.89 (d, J_{HH} = 8.0 Hz, 1H), 8.20 (t, J_{HH} = 8.5 Hz, 1H), 8.14 (d, J_{HH} = 6.5 Hz, 1H), 8.09 (d, J_{HH} = 8.5 Hz, 2H), 7.69−7.66 (m, 2H), 7.29 (s, 2H), 7.21 (s, 2H), 6.83 (d, J_{HH} = 4.0 Hz, 1H), 2.72 (t, J_{HH} = 6.0 Hz, 2H), 1.54−1.51 (m, 2H), 1.24−1.12 (m, 6H), 0.84 (t, J_{HH} = 7.0 Hz, 3H). ^{19}F NMR (376 MHz, DMSO-d_6, 298 K): δ −58.48 (s, 6F).

Synthesis of TF-12. With the procedure described for **TF-11**, the reaction of **L2** (175 mg, 0.32 mmol), $RuCl_3{\cdot}3H_2O$, (92 mg, 0.35 mmol), 2,6-bis(3-trifluoromethyl-1*H*-pyrazol-5-yl)pyridine (46 mg, 0.13 mmol), and 4-ethylmorpholine (0.04 mL, 0.35 mmol) afforded, after NaOH hydrolysis and subsequent acidification, **TF-12** as a brown solid product (99 mg, 36%).

Selected Spectral Data for ***TF-12****.* MS (FAB, ^{102}Ru): m/z 934 [M + H]$^+$. ^{1}H NMR (400 MHz, DMSO-d_6, 298 K): δ 9.21 (s, 1H), 9.15 (s, 1H), 9.00 (d, J_{HH} = 8.0 Hz, 1H), 8.97 (s, 1H), 7.97 (t, J_{HH} = 8.0 Hz, 1H), 7.89 (t, J_{HH} = 8.0 Hz, 1H), 7.73 (d, J_{HH} = 8.0 Hz, 2H), 7.62 (d, J_{HH} = 8.0 Hz, 1H), 7.32 (d, J_{HH} = 8.0 Hz, 1H), 7.11 (s, 2H), 6.78 (d, J_{HH} = 6 Hz, 1H), 6.11 (d, J_{HH} = 3.2 Hz, 1H), 5.38 (d, J_{HH} = 3.2 Hz, 1H), 2.57 (t, J_{HH} = 7.6 Hz, 2H), 1.50 (quin, J_{HH} = 7.6 Hz, 2H), 1.31 (m, 6H), 0.87 (t, J_{HH} = 6.8 Hz, 3H). ^{19}F NMR (376 MHz, DMSO-d_6, 298 K): δ −58.30 (s, 6F). Anal. Calcd for $C_{40}H_{30}F_6N_8O_4RuS{\cdot}2H_2O$: C, 49.54; N, 11.55; H, 3.53. Found: C, 49.64; N, 11.27; H, 3.51.

Synthesis of TF-13. With the procedure described for **TF-11**, the reaction of **L3** (137 mg, 0.23 mmol), $RuCl_3{\cdot}3H_2O$, (65 mg, 0.25 mmol), 2,6-bis(3-trifluoromethyl-1*H*-pyrazol-5-yl)pyridine (71 mg, 0.20 mmol), and KOAc (100 mg, 1.02 mmol) afforded, after NaOH hydrolysis and subsequent acidification, **TF-13** as a brown solid product (142 mg, 63%).

Selected Spectral Data for ***TF-13****.* MS (FAB, ^{102}Ru): m/z 993 [M + H]$^+$. ^{1}H NMR (400 MHz, DMSO-d_6, 298 K): δ 9.31 (s, 1H), 9.15 (s, 1H), 9.09 (s, 1H), 8.77 (d, J_{HH} = 8.4 Hz, 1H), 8.22 (t, J_{HH} = 7.2 Hz, 1H), 8.12 (d, J_{HH} = 7.6 Hz, 2H), 7.76 (d, J_{HH} = 5.6 Hz, 1H), 7.72 (s, 2H), 7.68 (d, J_{HH} = 6.0 Hz, 1H), 7.30 (s, 2H), 4.16 (m, 2H), 4.10 (m,

dx.doi.org/10.1021/ja300828f | J. Am. Chem. Soc. 2012, 134, 7488−7496

2H), 2.54 (t, J_{HH} = 7.2 Hz, 2H), 1.46−1.44 (m, 2H), 1.22−1.18 (m, 6H), 0.82 (t, J_{HH} = 6.8 Hz, 3H). ^{19}F NMR (376 MHz, DMSO-d_6, 298 K): δ −55.64 (s, 6F). Anal. Calcd for $C_{42}H_{32}F_6N_8O_6RuS{\cdot}2H_2O$: C, 49.08; N, 10.90; H, 3.53. Found: C, 49.09; N, 10.89; H, 3.86.

Synthesis of TF-14. With the procedure described for **TF-11**, complex **TF-14** (124 mg) was obtained in 69% yield from the sequential reaction of ligand **L4**, $RuCl_3{\cdot}3H_2O$, and 2,6-bis(3-trifluoromethyl-1*H*-pyrazol-5-yl)pyridine followed by NaOH hydrolysis and acidification.

Selected Spectral Data for ***TF-14****.* MS (FAB, ^{102}Ru): m/z 993 [M + H]$^+$. ^{1}H NMR (400 MHz, DMSO-d_6, 298 K): δ 9.21 (s, 1H), 9.16 (s, 1H), 9.02 (d, J_{HH} = 8.0 Hz, 1H), 8.98 (s, 1H), 7.97 (q, J_{HH} = 7.2 Hz, 2H), 7.83 (m, 2H), 7.63 (d, J_{HH} = 4.8 Hz, 1H), 7.29 (d, J_{HH} = 7.2 Hz, 1H), 7.16 (s, 2H), 6.82 (d, J_{HH} = 6.0 Hz, 1H), 4.06 (s, 2H), 3.68 (s, 2H), 2.39−2.30 (m, 2H), 1.41−1.39 (m, 2H), 1.39−1.25 (m, 6H), 0.91−0.82 (m, 3H). ^{19}F NMR (376 MHz, DMSO-d_6, 298 K): δ −58.24 (s, 6F). Anal. Calcd for $C_{42}H_{32}F_6N_8O_6RuS{\cdot}2H_2O$: C, 49.08; N, 10.90; H, 3.53. Found: C, 49.41; N, 10.59; H, 3.69.

DFT Calculations. All of the calculations were performed using the Gaussian 09 program.[28] For ground-state geometry optimization of **TF-11** and **TF-12**, density functional theory (DFT) with the B3LYP hybrid functional was used.[29,30] The basis set consisted of the 6-31G(d)[31] set for H, C, N, O, and S atoms and the LANL2DZ basis set for the Ru atom, and a relativistic effective core potential (ECP) was applied to the inner core electrons of Ru.[32−34] For the simulation of the absorption spectrum, the vertical excitation from the optimized ground-state structure was calculated at the time-dependent DFT (TD-DFT) level using the same hybrid functional (B3LYP) and basis set (LANL2DZ for Ru, 6-31G(d) for ligand atoms). All of the calculations included solvation effects [with *N*,*N*-dimethylformamide (DMF) as the solvent] using the conductor-like polarizable continuum model (C-PCM).[35−38]

Device Fabrication. The fluorine-doped tin oxide (FTO) glass used as current collector (3.2 mm thickness, sheet resistance of 9 Ω/cm^2, Pilkington) was first cleaned for 30 min in a detergent solution using an ultrasonic bath and then rinsed with water and ethanol. After treatment in a UV−O_3 system for 15 min (PSD series UV−ozone cleaning, Novascan Technologies, Inc.), the FTO glass plates were immersed in a 40 mM aqueous $TiCl_4$ solution at 70 °C for 30 min and then washed with water and ethanol. The photoanodes composed of nanocrystalline TiO_2 were prepared using literature procedures.[39] For optimized DSC devices, TiO_2 electrodes with a thickness of 15 μm were deposited onto transparent conducting glass over which a scattering layer with a thickness of 7 μm containing 400 nm TiO_2 particles (PST-400, JGC Catalysts and Chemicals, Japan) was screen-printed (0.16 cm^2 active area). For transient absorption spectroscopy (TAS) measurements, 7 μm thick TiO_2 electrodes (1 cm^2 active area) were used. The TiO_2 film thickness was measured by α-step IQ surface profile (KLA Tencor). The TiO_2 electrodes were heated under an air flow at 325 °C for 30 min and then at 375 °C for 5 min, 450 °C for 15 min, and 500 °C for 30 min. The TiO_2 electrodes were treated with a 40 mM aqueous solution of $TiCl_4$, sintered at 70 °C for 30 min, and then washed with water and ethanol. The electrodes were heated again at 500 °C for 30 min and left to cool to 80 °C before being dipped into the dye solution (0.3 mM in ethanol with 15 mM chenodeoxycholic acid as a coadsorbent) for 18 h at 25 °C. Next, the Pt counter electrodes were spin-coated onto the FTO plates using a solution of H_2PtCl_6 (2 mg of Pt in 1 mL isopropyl alcohol) and sintered at 400 °C for 15 min. The dye-sensitized TiO_2 electrodes were assembled with the Pt counter electrodes by inserting a hot-melt Surlyn film (Meltonix 1170-25, 25 μm, Solaronix) as spacer between the electrodes and then heated at 130 °C. The electrolyte consisted of 0.6 M 1,2-dimethyl-3-propylimidazolium iodide (DMPII), 0.05 M of iodine, 0.5 M *tert*-butylpyridine (TBP), and 0.1 M of LiI in acetonitrile, which was then injected into the cell through a drilled hole at the counter electrode. Finally, the hole was sealed using a hot-melt Surlyn film and a cover glass. To reduce scattered light from the edge of the glass electrodes of the dyed TiO_2 layer, all of the devices were covered with a light-shading mask with a size of 0.6 cm × 0.6 cm.[40]

Photovoltaic Characterization. Photovoltaic measurements were recorded with a Newport Oriel class A solar simulator (model 91159) equipped with a class A 150 W xenon light source powered by a Newport power supply (model 69907). The light output (area: 2 in. × 2 in.) was calibrated to AM 1.5 using a Newport Oriel correction filter to reduce the spectral mismatch in the 350−750 nm region to less than 4%. The power output of the lamp was measured to 1 Sun (100 mW cm^{-2}) using a certified Si reference cell (SRC−1000−TC−QZ, VLSI standard, S/N 10510-0031). The current−voltage characteristics of each cell were obtained by applying an external potential bias to the cell and measuring the generated photocurrent with a Keithley digital source meter (model 2400). The incident photon-to-current conversion efficiency (IPCE) was measured as a function of excitation wavelength using the incident light from a 300 W xenon lamp (model 6258, Newport Oriel), which was focused through an Oriel Cornerstone 260 1/4 m monochromator (model 74100) onto the photovoltaic cell under measurement. The light intensities were calibrated with a Newport 818 UV detector. Photovoltaic performance was measured using a metal mask with an aperture area of 0.36 cm^2.

Transient Photovoltage and Charge Extraction Measurements. Transient photovoltage (TPV) and charge extraction (CE) measurements were carried out on optimized 0.16 cm^2 DSC devices using a system similar to that employed by O'Regan et al.[41]

Electrical Impedance Spectroscopy Measurements. Electrical impedance spectroscopy (EIS) experiments were carried out using a PARSTAT 2273 electrochemical workstation (AMETEK Princeton Applied Research, Oak Ridge, TN) with a frequency range of 0.05−10^6 Hz and a potential modulation of 10 mV.

Transient Absorption Spectroscopy Measurements. TAS measurements were carried out on 1 cm^2 DSC devices using a system similar to that used by Durrant and co-workers.[42]

Stability Test. The photoanodes of the devices employed in this study were composed of a 15 μm transparent TiO_2 thin film and a 5 μm thick layer of 400 nm TiO_2 particles. A 370 nm cutoff long-pass filter film was attached on the cell surface during illumination. The cell was irradiated under a Suntest CPS+ lamp (ATLAS GmbH, 100 mW cm^{-2}) during visible-light soaking at 60 °C. The electrolyte consisted of 1.0 M 1,3-dimethylimidazolium iodide (DMII), 0.15 M iodine, 0.1 M guanidinium thiocyanate (GNCS), 0.1 M LiI, and 0.5 M *N*-butyl-1*H*-benzimidazole (NBB) in 3-methoxypropionitrile (MPN).

RESULTS AND DISCUSSION

Sensitizer Synthesis and Characterization. The chemical structures of the novel TF Ru(II) sensitizers are shown in Scheme 2. The synthesis of these Ru(II) complexes required

Scheme 2. Structures of Ru(II) sensitizers TF-11−14

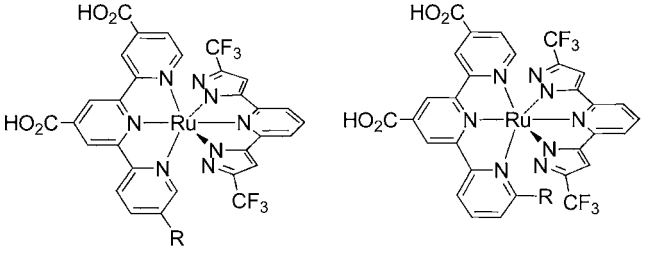

TF-11, R = 5-(2-hexylthiophene) **TF-12**, R = 5-(2-hexylthiophene)
TF-13, R = 5-(2-hexyl-EDOT) **TF-14**, R = 5-(2-hexyl-EDOT)

the use of dicarboxyterpyridine chelates with either a 2-hexylthiophene or 2-hexyl-3,4-ethylenedioxythiophene (2-hexyl-EDOT) functional group attached at the 5- or 6-position of one terminal pyridyl unit. Their synthesis was achieved in reasonable yield from the Pd-catalyzed coupling of diethyl 6-bromo-2,2′-bipyridine-4,4′-dicarboxylate and the corresponding tri-*n*-butyltin reagents (Scheme 3).[43] Diethyl 6-bromo-2,2′-

dx.doi.org/10.1021/ja300828f | J. Am. Chem. Soc. 2012, 134, 7488−7496

Scheme 3. Simplified Synthetic Protocol for the Dicarboxyterpyridine Chelates

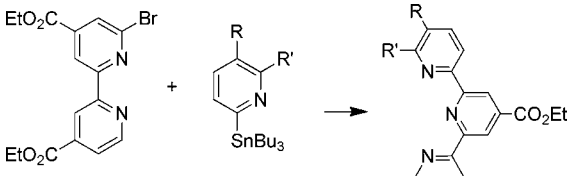

L1, **L2**: R, R'; R', R = 5-(2-hexylthiophene), H
L3, **L4**: R, R'; R', R = 5-(2-hexyl-EDOT), H

bipyridine- 4,4′-dicarboxylate was made using a modified procedure that was originally intended for double bromination of diethyl 2,2′-bipyridine-4,4′-dicarboxylate,[44] while each of the tri-*n*-butyltin reagents were prepared using literature methods. After this, the addition of the dicarboxyterpyridine ligand and 2,6-bis(3-trifluoromethyl-1*H*-pyrazol-5-yl)pyridine to the $RuCl_3 \cdot H_2O$ reagent resulted in the formation of the ethoxycarbonyl derivatives, and subsequent NaOH-catalyzed ester hydrolysis afforded the Ru(II) sensitizers **TF-11**−**14** in high yield. The identities of all of the chelating ligands and the Ru(II) sensitizers were verified by routine mass analysis, ^{1}H and ^{19}F NMR spectroscopies, and/or elemental analysis. Relevant synthetic procedures and spectroscopic data for the chromophoric ligands and their intermediates are all given in the Supporting Information.

The absorption spectra of these TF dyes in DMF solution are shown in Figure 1a, together with that of **N749** for comparison. Their pertinent photophysical and electrochemical properties are summarized in Table 1. In contrast to **N749** with its broad absorption band centered around 600 nm, the TF complexes show narrower and more intense absorption bands centered at 510 nm. These bands are mainly assigned to the metal-to-ligand charge-transfer (MLCT) transition to the dicarboxyterpyridine ligand. Furthermore, for **TF-11** and **TF-13** there exist intense signals at 363 and 389 nm, respectively, that are assigned to the intraligand $\pi-\pi^*$ transition associated with the added thiophene and EDOT pendant groups. This assignment is further indicated by the lack of any similar transitions for **TF-12** and **TF-14**, for which the respective thiophene and EDOT pendant groups are believed to adopt a vertical orientation relative to the terpyridine chelate because of the excessive steric congestion exerted by the adjacent 2,6-bis(5-pyrazolyl)pyridine chelate.

Further salient differences with respect to the absorption spectrum of **N749** are that all of the TF dyes exhibit broad absorption at longer wavelengths with peak maxima centered at 685−712 nm and a shoulder extending to 800 nm, which are probably attributable to the spin-forbidden ^{3}MLCT transition. Notably, the intense MLCT band at 606 nm in **N749** is substantially suppressed in all of the **TF-11**−**14** dyes, which could be due to the lack of thiocyanate. These spectral assignments are further supported by theoretical calculations. With **TF-11** and **TF-12** as the paradigm, Figure 1b depicts the selected optically active electronic transitions obtained from TD-DFT C-PCM calculations in DMF as the medium. The corresponding frontier orbitals for some of the major transitions are also depicted in Figure 1b. The calculated energy levels, oscillator strengths, and orbital transition analyses are listed in Tables S1 and S2 and Figure S1 in the Supporting Information. According to these calculations, the spin density propagation for the lower-lying electronic transitions (>550

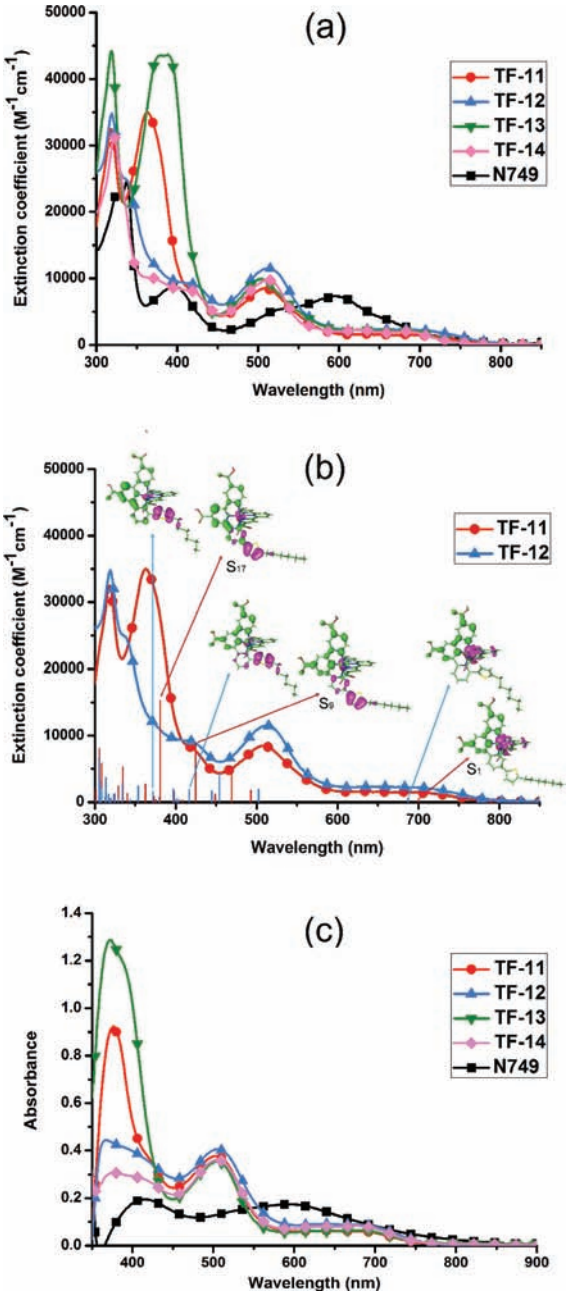

Figure 1. (a) Absorption spectra of the **TF** dyes and **N749** in DMF. (b) The absorption spectra of **TF-11** and **TF-12** and the corresponding optically active electronic transitions with the associated frontier orbitals (oscillator strength >0.01; red and blue bars are for **TF-11** and **TF-12**, respectively, while occupied and unoccupied orbitals are shown in magenta and green, respectively). (c) Absorption spectra for all samples taken on a 6 μm mesoporous TiO_2 thin film.

nm) is mainly derived from the Ru(II) d_π orbital and bonding orbitals of the pyrazolates to the antibonding orbitals of the dicarboxyterpyridine chelate. A localized intraligand $\pi-\pi^*$ transition appears, as evidenced by the frontier orbital analyses and high oscillator strength, in the 350−470 nm region, corresponding to the S_6 and/or higher excited states. Special attention was paid to the absorption bands in the higher-energy 370−430 nm region, for which the frontier orbital analyses indicate that the electron density is in part distributed around the thiophene fragment (see the electron−hole densities at 424 and 416 nm for **TF-11** and **TF-12** respectively, in Figure 1b),

dx.doi.org/10.1021/ja300828f | *J. Am. Chem. Soc.* 2012, 134, 7488−7496

Table 1. Photophysical and Electrochemical Data for TF-11−14 and N749

dye	λ_{abs}/nm (ε/L mol^{-1} cm^{-1})[a]	E°_{ox} (V)	E_{0-0} (V)[b]	$E^{\circ *}$ (V)[c]
TF-11	363 (35047), 512 (8483), 712 (1456)	0.93	1.68	−0.75
TF-12	319 (34790), 513 (11568), 704 (2228)	0.91	1.71	−0.80
TF-13	319 (44183), 389 (43643), 506 (9918), 688 (2073)	0.90	1.70	−0.80
TF-14	322 (31275), 514 (9817), 685 (2024)	0.88	1.66	−0.78
N749	338(24519), 398 (8847), 598 (7330)	0.89	1.66	−0.77

[a]Absorption and emission spectra were measured in DMF solution. [b]E_{0-0} was determined from the intersection of the absorption peak and the tangent of the emission peak in DMF. [c]$E^{\circ *}$ was calculated as $E^{\circ}_{ox} - E_{0-0}$.

manifesting the contribution of the pendant groups to the harvesting of solar energy and hence the overall DSC performance (see below).

Cyclic voltammetry was conducted to examine whether the oxidation potentials of this series of TF sensitizers match the redox potential of the electrolyte. This would ensure that there is enough driving energy for dye regeneration to occur and also verify that the excited-state oxidation potentials, $E^{\circ *}_{ox}$, are more negative than the conduction band of TiO_2 for efficient electron injection. All of the oxidation potentials were measured in DMF with 0.1 M $TBAPF_6$ at a scan rate of 50 mV s^{-1} (vs NHE). It was calibrated with ferrocene/ferrocenium as the reference and converted to NHE by addition of 0.63 V. As shown in Table 1, their electrochemical oxidation potentials E°_{ox} appeared in the range 0.93−0.88 V vs NHE, which is notably larger than that of the I^-/I_3^- redox couple (ca. 0.4 V vs NHE). Alternatively, the excited-state oxidation potentials $E^{\circ *}_{ox}$, which ranged from −0.75 to −0.80 V, are sufficiently more negative than the conduction-band edge of the TiO_2 electrode (ca. −0.5 V vs NHE).

Device Characterization. The performance of these sensitizers in DSC devices was examined. The composition of the electrolyte (0.6 M DMPII, 0.05 M iodine, 0.5 M TBP, and 0.1 M LiI in acetonitrile) was essentially identical to that employed previously for the **N749** sensitizer,[15] except that we reduced the I_2 concentration from 0.1 to 0.05 M with the aim of suppressing charge recombination and boosting the device efficiency. The IPCEs of these DSC dyes are shown in Figure 2a. The steep rise of the IPCE action spectra for all of the TF complexes started at ∼810 nm, matching well with their absorption spectra on TiO_2 thin films (see Figure 1c). Excellent IPCE performances were observed in the visible wavelength region (450−700 nm). It is notable that except for **TF-12**, which exhibits a maximum IPCE of 60% between 600 and 720 nm, the other TF sensitizers show inferior IPCE values of ∼50% in this region. For a comparison, DSCs fabricated using **N749** showed a maximum IPCE at 450−610 nm and a steadily decreasing IPCE at longer wavelengths and beyond 900 nm (see Figure 2a). For the EDOT-functionalized sensitizers **TF-13** and **TF-14**, although greater extinction coefficients were observed, both still exhibited lower short-circuit current density (J_{SC}), open-circuit voltage (V_{OC}), and overall conversion efficiency (η) values. It is believed that the inferior efficiencies are due to the greater molecular sizes, which then prohibit the effective penetration into the interior of the TiO_2 electrode, as shown by the slightly reduced dye loading (Table 2). Relevant studies of the trade-off between geometric enlargement and cell efficiency have been well-documented.[45,46] Furthermore, as we

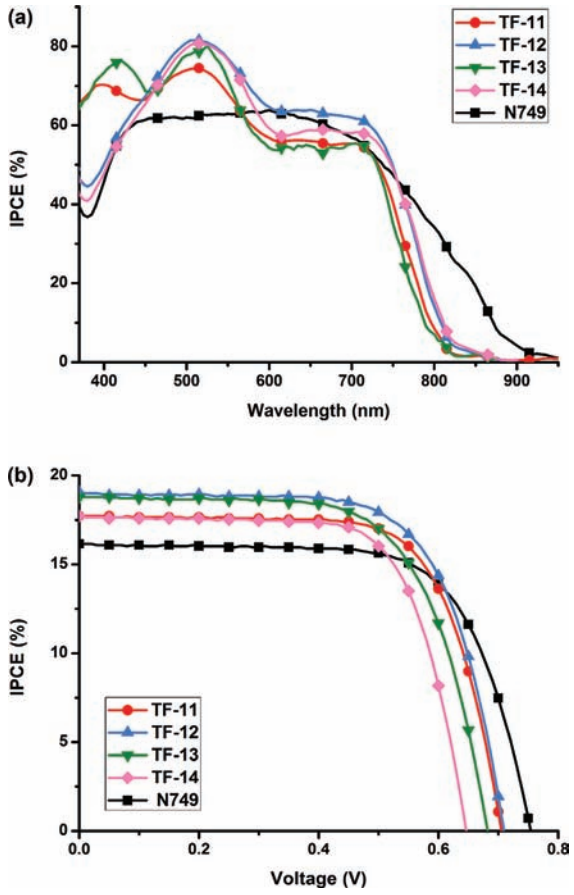

Figure 2. (a) Incident photon-to-current conversion efficiency (IPCE) spectra and (b) photocurrent density−voltage curves of DSC devices sensitized with **TF** dyes and the reference **N749**.

Table 2. Performance of DSCs Measured under AM1.5G One-Sun Irradiation[a]

dye	J_{SC} (mA cm^{-2})	V_{OC} (V)	FF	η (%)	dye loading (10^{-8} mol cm^{-2})[c]
TF-11	17.7	0.710	0.699	8.80	7.53
TF-12	19.0	0.710	0.681	9.21	5.70
	21.5	0.710	0.683	10.4[b]	
TF-13	18.7	0.680	0.668	8.53	3.99
TF-14	17.7	0.650	0.697	8.05	3.85
N749	16.1	0.750	0.694	8.40	3.78

[a]Except for those with specific remarks, all of the devices were fabricated using a 15 + 7 μm TiO_2 anode with a 4 mm × 4 mm working area, an electrolyte that consists of 0.6 M DMPII, 0.05 M I_2, 0.5 M TBP, and 0.1 M LiI in acetonitrile. Also, all of the as-prepared devices were covered by a 6 mm × 6 mm shadow mask for the performance measurement. [b]Measured in the absence of the shadow mask. [c]The dye loading on 6 μm TiO_2 films was determined by desorbing the dye into a 0.1 M TBAOH solution in 1:1 (v/v) MeOH/H_2O and then performing the UV/vis spectral analysis.

observed previously,[47] the presence of EDOT groups in the sensitizers can lower V_{OC} because of an acceleration of recombination between electrons in TiO_2 and the oxidized electrolyte.

Figure 2b shows the photocurrent density−voltage curves of the DSC devices recorded under AM1.5G simulated sunlight at a light intensity of 100 mW cm^{-2}; the data is detailed in Table 2. **N749** showed J_{SC}, V_{OC}, fill factor (FF), and η values of 16.1

dx.doi.org/10.1021/ja300828f | J. Am. Chem. Soc. 2012, 134, 7488−7496

mA cm^{-2}, 750 mV, 0.694, and 8.40%, respectively. It should be noted that the conversion efficiency is lower than those reported by Wang (10.5%)[48] and Han (11.1%).[49,50] However, the TF-sensitized solar cells were endowed with better efficiencies. For instance, **TF-11** gave J_{SC} = 17.7 mA cm^{-2}, V_{OC} = 710 mV, and FF = 0.699, corresponding to an overall conversion efficiency of η = 8.80%, while the **TF-12** sensitizer gave the best performance data, J_{SC} = 19.0 mA cm^{-2}, V_{OC} = 710 mV, FF = 0.681, and η = 9.21%. All these TF sensitizers showed higher current densities (17.7−19.0 mA cm^{-2}) than **N749** (16.1 mA·cm^{-2}), reflecting the increased absorption and light-harvesting efficiency upon introduction of the π-conjugated pendant groups.

To investigate the recombination processes occurring in these devices, TPV, CE, EIS, and TAS measurements were carried out. CE is a tool to measure electron densities in functioning devices, whereas TPV and EIS are used to measure the lifetimes of TiO_2 electrons in devices under operational conditions and their recombination with oxidized species present in the electrolyte. TAS on the other hand can be used to measure the charge recombination reaction between photoinjected electrons in TiO_2 and dye cations in the absence of electrolyte and also the regeneration of these dye cations in the presence of electrolyte.

Differences in V_{OC} between cells can generally be explained either by shifts in the TiO_2 conduction-band edge (manifested by the shift of the exponential distribution of experimental data measured by CE) and/or by TiO_2 recombination lifetimes (investigated via TPV measurements). The CE and TPV data for devices composed of the TF sensitizers as well as for **N749** are shown in Figure 3. The DSC devices showed negligible differences in charge densities (Figure 3a) as measured by CE, indicating that the conduction-band potential is similar in all cases. Therefore, shifts in the Fermi level cannot explain the differences in voltage observed in these devices. On the other hand, electron lifetimes measured at identical electron densities using TPV measurements (Figure 3b) fit well with the cell voltages listed in Table 2, where longer electron lifetimes correspond to larger device voltages. From Figure 3b, the electron lifetimes follow the order **N749** > **TF-12** > **TF-11** > **TF-13** > **TF-14**.

To complement the TPV measurements, EIS measurements were also conducted to investigate the electron lifetimes in these devices. Figure 4 shows the Nyquist plots measured under dark conditions at a forward bias of 0.7 V. Two semicircles from left to right in the Nyquist plot are visible and represent the impedances of the charge transfer on the Pt counter electrode (R_{Pt}, smaller circles) and the charge recombination at the TiO_2/dye/electrolyte interface (R_r, larger circles).[51] The radii of the second series of semicircles indicates R_r to decrease in the order **N749** > **TF-12** > **TF-11** > **TF-13** > **TF-14**. A smaller R_r value in theory means faster charge recombination between electrons in TiO_2 and electron acceptors in the electrolyte and thus a shorter TiO_2 electron lifetime. Therefore, the trends observed for the electron lifetimes extracted from the TPV and EIS measurements are identical and furthermore are consistent with the trend in V_{OC} values measured for these devices. We note that a correlation of the electron lifetime with the cell V_{OC} has also been observed for DSC devices based on organic donor−acceptor dyes[52−54] and thiocyanate-containing Ru(II) sensitizers,[55] but we present such a correlation for the first time here for a series of thiocyanate-free Ru(II) sensitizers. Finally, we point out that

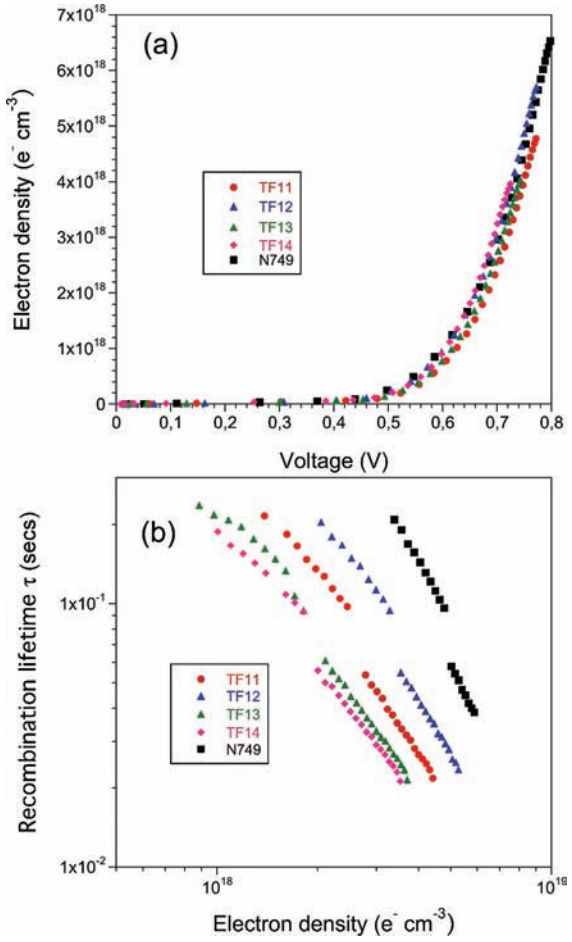

Figure 3. (a) TiO_2 electron density as a function of voltage deduced from CE measurements and (b) recombination lifetime τ as a function of TiO_2 electron density deduced from TPV measurements for DSC devices containing TF sensitizers and the reference **N749**. The cell voltage was induced via illumination from a series of LEDs.

both the TPV and EIS measurements indicate that devices based on the EDOT-functionalized sensitizers (**TF-13** and **TF-14**) have shorter lifetimes than their thiophene-functionalized counterparts (**TF-11** and **TF-12**). We also observed this in a

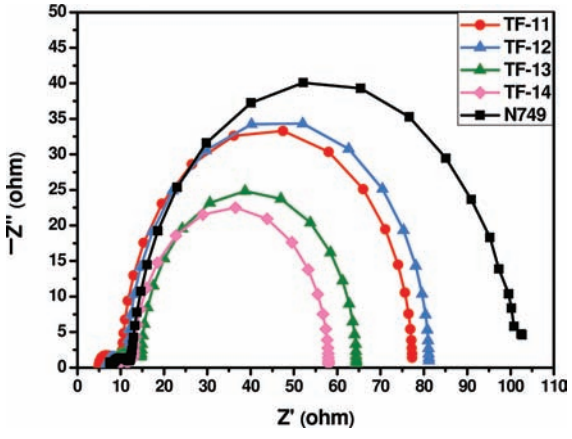

Figure 4. Electrochemical impedance spectra measured under dark conditions at a forward bias of 0.7 V for DSC devices containing TF sensitizers and the reference **N749**.

dx.doi.org/10.1021/ja300828f | J. Am. Chem. Soc. 2012, 134, 7488−7496

previous study involving organic dyes that contained similar functional groups.[47]

TAS measurements investigating the charge recombination dynamics in DSC devices were performed for the reference dye **N749** and for **TF-12** in the presence and absence of electrolyte (Figure 5). The dynamics for the other TF dyes can be found

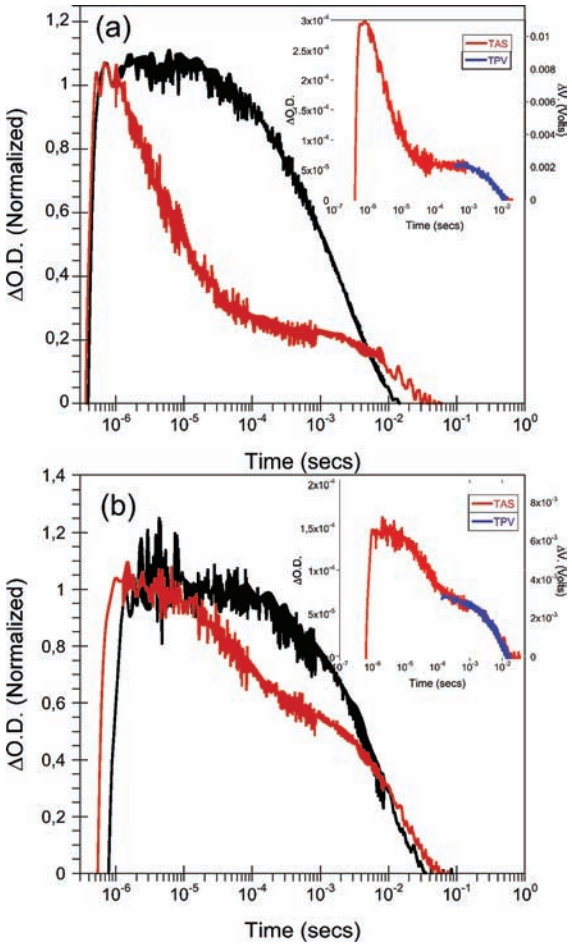

Figure 5. Transient absorption kinetics of (a) **N749** and (b) **TF-12** DSC devices in the presence (red) and absence (black) of redox electrolyte. The insets show comparisons of the TAS kinetics (red) and TPV decay (blue), both recorded under AM1.5G one-sun illumination. All of the TAS and TPV transients were recorded using laser excitation pulses of 628 nm (**N749**) or 500 nm (**TF-12**). The TAS kinetics was recorded at 800 nm.

in the Supporting Information. In the absence of electrolyte, both **N749** and **TF-12** showed multiexponential behavior very similar to that observed previously in studies involving Ru(II) polypyridine complexes.[42] In the presence of electrolyte, the dynamics becomes biphasic as the dye cations are regenerated by the iodide in the electrolyte, resulting in the appearance of a long-lived signal assigned to electrons in TiO_2 and/or $I_2^{\bullet-}$.[56] The dynamics for **N749** are similar to those measured previously, indicating efficient regeneration.[57] For **TF-12**, however, the loss of the cation signal due to regeneration is not nearly as rapid. This behavior was the same for all of the TF dyes measured and indicates that regeneration in the case of the TF dyes is not as efficient as for **N749**. This difference cannot be due to reaction driving force, as electrochemical measurements on the TF dyes indicated ground-state potentials similar to that of **N749** (0.8 V vs NHE). We tentatively attribute the difference in regeneration to the rather different molecular structures of the TF dyes relative to **N749**. The bulky ancillary tridentate terpyridine ligand in the TF series would be expected to hinder the interaction between iodide and Ru(II) where the cation is centered. For **N749**, the thiocyanate groups do not present such an obstacle. Moreover, as already mentioned, the thiocyanate groups take an active part in regeneration.[58] In any case, the slower regeneration did not appear to have any significant effect on device performance, as the TF dyes showed outstanding efficiencies as demonstrated in Table 2.

The insets in Figure 5 show the TAS kinetics for **N749** and **TF-12** devices under AM1.5G one-sun illumination (provided by a series of LEDs) under open-circuit conditions along with TPV decays recorded under almost identical conditions following excitation with a laser pulse. It is clear that the decay of the long-lived TAS signal and the TPV decay correspond rather well. It is therefore reasonable to conclude that the long-lived signal in the TAS dynamics is that of electrons in the TiO_2.

The long-term stability of a device is a crucial parameter for its practical application in DSCs. The device based on **TF-12** was fabricated by using a double-layered TiO_2 film (15 + 5 μm) with a low-volatility electrolyte based on MPN as the solvent. After a 1000 h testing period at 60 °C under one-sun light soaking, the photovoltaic parameters J_{SC}, V_{OC}, and FF of the **TF-12**-based cell changed only slightly from the initial values (Figure 6). As a result, η retained 98% of its initial value; it

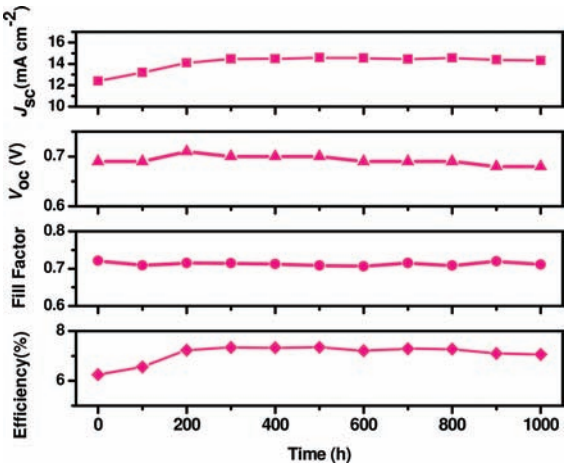

Figure 6. Evolution of the solar cell parameters of **TF-12** measured under AM1.5G sunlight soaking at 60 °C. A 405 nm cutoff long-pass filter was put on the cell surface during illumination. The efficiency decline was measured to be 2.3%. The electrolyte was 1.0 M DMII, 0.15 M iodine, 0.1 M GNCS, 0.1 M LiI, and 0.5 M NBB in MPN.

should be noted that a small drop of 30 mV in V_{OC} is balanced by an increase in J_{SC} due perhaps to the long-term re-equilibrium and hence slight redistribution of dyes adsorbed on TiO_2 to avoid, in part, aggregation.

CONCLUSION

To sum up, we have reported a new series of bis-tridentate Ru(II) sensitizers (**TF-11**–**14**) in which a π-conjugated thiophene pendant group has been strategically added onto the dicarboxyterpyridine chelating ligand at the 5- or 6-position of the terminal pyridyl unit. This pendant group serves as an antenna to harvest solar energy, increasing the light-harvesting efficiency as demonstrated by absorption and IPCE spectra and

dx.doi.org/10.1021/ja300828f | J. Am. Chem. Soc. 2012, 134, 7488–7496

verified using DFT calculations. In addition, DSC devices showed high overall conversion efficiencies. Devices based on **TF-12** reached a short-circuit photocurrent of 19.0 mA cm^{-2}, an open-circuit voltage of 0.71 V, and a fill factor of 0.68, affording an overall conversion efficiency of 9.21%, which is higher than that of the reference **N749** device. A clear correlation between the device V_{OC} and the cell electron lifetime under working conditions was also observed for these sensitizers using both electrical impedance and transient photovoltage measurements. The designated bis-tridentate configuration firmly stabilizes the corresponding Ru(II) sensitizers, as evidenced by the fact that a **TF-12** device retained ≥98% of its initial efficiency after a 1000 h testing period at 60 °C under one-sun light soaking. We believe that the degradation even over this time span could be avoided by improving the sealing process, showing the great prospects of these designs for use in dye-sensitized solar cells.

■ ASSOCIATED CONTENT

Ⓢ Supporting Information

Synthetic procedures and the associated spectral data for all of the chromophoric ligands, figures showing the absorption spectra and selected electronic transitions of **TF-11** and **TF-12** obtained using the TD-DFT C-PCM calculations in DMF, and figures containing TAS and TPV decays. This material is available free of charge via the Internet at http://pubs.acs.org.

■ AUTHOR INFORMATION

Corresponding Author

ychi@mx.nthu.edu.tw; epalomares@iciq.es; chop@ntu.edu.tw

Author Contributions

⊥K.-L.W. and C.-H.L. contributed equally.

Notes

The authors declare no competing financial interest.

■ ACKNOWLEDGMENTS

This work was supported by the National Science Council of Taiwan. We are also grateful to the National Center for High-Performance Computing for computer time and facilities. E.P. is grateful for the financial support from ICIQ, ICREA, and the Spanish MICINN Projects CTQ2010-18859 and CONSOLIDER CDS-0007 HOPE-2007 and also thanks the EU for the ERCstg Polydot and the Catalan Government for the 2009-SGR-207 Project. J.N.C. thanks the MICINN for the Juan de la Cierva Fellowship.

■ REFERENCES

(1) Peter, L. M. *J. Phys. Chem. Lett.* **2011**, *2*, 1861.
(2) Clifford, J. N.; Martinez-Ferrero, E.; Viterisi, A.; Palomares, E. *Chem. Soc. Rev.* **2011**, *40*, 1635.
(3) Yum, J.-H.; Chen, P.; Grätzel, M.; Nazeruddin, M. K. *ChemSusChem* **2008**, *1*, 699.
(4) Hamann, T. W.; Jensen, R. A.; Martinson, A. B. F.; Van Ryswyk, H.; Hupp, J. T. *Energy Environ. Sci.* **2008**, *1*, 66.
(5) Goncalves, L. M.; de Zea Bermudez, V.; Ribeiro, H. A.; Mendes, A. M. *Energy Environ. Sci.* **2008**, *1*, 655.
(6) Anandan, S. *Sol. Energy Mater. Sol. Cells* **2007**, *91*, 843.
(7) Grätzel, M. *Inorg. Chem.* **2005**, *44*, 6841.
(8) Hagfeldt, A.; Boschloo, G.; Sun, L.; Kloo, L.; Pettersson, H. *Chem. Rev.* **2010**, *110*, 6595.
(9) Grätzel, M. *Acc. Chem. Res.* **2009**, *42*, 1788.
(10) Robertson, N. *Angew. Chem., Int. Ed.* **2006**, *45*, 2338.
(11) Ooyama, Y.; Harima, Y. *Eur. J. Org. Chem.* **2009**, 2903.
(12) Mishra, A.; Fischer, M. K. R.; Bauerle, P. *Angew. Chem., Int. Ed.* **2009**, *48*, 2474.
(13) Ning, Z.; Fu, Y.; Tian, H. *Energy Environ. Sci.* **2010**, *3*, 1170.
(14) Reynal, A.; Palomares, E. *Eur. J. Inorg. Chem.* **2011**, 4509.
(15) Nazeeruddin, M. K.; Pechy, P.; Renouard, T.; Zakeeruddin, S. M.; Humphry-Baker, R.; Comte, P.; Liska, P.; Cevey, L.; Costa, E.; Shklover, V.; Spiccia, L.; Deacon, G. B.; Bignozzi, C. A.; Grätzel, M. *J. Am. Chem. Soc.* **2001**, *123*, 1613.
(16) Wadman, S. H.; Kroon, J. M.; Bakker, K.; Lutz, M.; Spek, A. L.; van Klink, G. P. M.; van Koten, G. *Chem. Commun.* **2007**, 1907.
(17) Wadman, S. H.; Kroon, J. M.; Bakker, K.; Havenith, R. W. A.; van Klink, G. P. M.; van Koten, G. *Organometallics* **2010**, *29*, 1569.
(18) Bessho, T.; Yoneda, E.; Yum, J.-H.; Guglielmi, M.; Tavernelli, I.; Imai, H.; Rothlisberger, U.; Nazeeruddin, M. K.; Grätzel, M. *J. Am. Chem. Soc.* **2009**, *131*, 5930.
(19) Bomben, P. G.; Gordon, T. J.; Schott, E.; Berlinguette, C. P. *Angew. Chem., Int. Ed.* **2011**, *50*, 10682.
(20) Bomben, P. G.; Theriault, K. D.; Berlinguette, C. P. *Eur. J. Inorg. Chem.* **2011**, 1806.
(21) Robson, K. C. D.; Koivisto, B. D.; Yella, A.; Sporinova, B.; Nazeeruddin, M. K.; Baumgartner, T.; Grätzel, M.; Berlinguette, C. P. *Inorg. Chem.* **2011**, *50*, 5494.
(22) Chi, Y.; Chou, P.-T. *Chem. Soc. Rev.* **2007**, *36*, 1421.
(23) Chen, B.-S.; Chen, K.; Hong, Y.-H.; Liu, W.-H.; Li, T.-H.; Lai, C.-H.; Chou, P.-T.; Chi, Y.; Lee, G.-H. *Chem. Commun.* **2009**, 5844.
(24) Chen, K.; Hong, Y.-H.; Chi, Y.; Liu, W.-H.; Chen, B.-S.; Chou, P.-T. *J. Mater. Chem.* **2009**, *19*, 5329.
(25) Wu, K.-L.; Hsu, H.-C.; Chen, K.; Chi, Y.; Chung, M.-W.; Liu, W.-H.; Chou, P.-T. *Chem. Commun.* **2010**, *46*, 5124.
(26) Chou, C.-C.; Wu, K.-L.; Chi, Y.; Hu, W.-P.; Yu, S. J.; Lee, G.-H.; Lin, C.-L.; Chou, P.-T. *Angew. Chem., Int. Ed.* **2011**, *50*, 2054.
(27) Yang, S.-H.; Wu, K.-L.; Chi, Y.; Cheng, Y.-M.; Chou, P.-T. *Angew. Chem., Int. Ed.* **2011**, *50*, 8270.
(28) Frisch, M. J.; Trucks, G. W.; Schlegel, H. B.; Scuseria, G. E.; Robb, M. A.; Cheeseman, J. R.; Scalmani, G.; Barone, V.; Mennucci, B.; Petersson, G. A.; Nakatsuji, H.; Caricato, M.; Li, X.; Hratchian, H. P.; Izmaylov, A. F.; Bloino, J.; Zheng, G.; Sonnenberg, J. L.; Hada, M.; Ehara, M.; Toyota, K.; Fukuda, R.; Hasegawa, J.; Ishida, M.; Nakajima, T.; Honda, Y.; Kitao, O.; Nakai, H.; Vreven, T.; Montgomery, J. A.; Peralta, J. E.; Ogliaro, F.; Bearpark, M.; Heyd, J. J.; Brothers, E.; Kudin, K. N.; Staroverov, V. N.; Kobayashi, R.; Normand, J.; Raghavachari, K.; Rendell, A.; Burant, J. C.; Iyengar, S. S.; Tomasi, J.; Cossi, M.; Rega, N.; Millam, J. M.; Klene, M.; Knox, J. E.; Cross, J. B.; Bakken, V.; Adamo, C.; Jaramillo, J.; Gomperts, R.; Stratmann, R. E.; Yazyev, O.; Austin, A. J.; Cammi, R.; Pomelli, C.; Ochterski, J. W.; Martin, R. L.; Morokuma, K.; Zakrzewski, V. G.; Voth, G. A.; Salvador, P.; Dannenberg, J. J.; Dapprich, S.; Daniels, A. D.; Farkas, O.; Foresman, J. B.; Ortiz, J. V.; Cioslowski, J.; Fox, D. J. *Gaussian 09*, revision B.01; Gaussian, Inc.: Wallingford, CT, 2009.
(29) Becke, A. D. *J. Chem. Phys.* **1993**, *98*, 5648.
(30) Lee, C.; Yang, W.; Parr, R. G. *Phys. Rev. B* **1988**, *37*, 785.
(31) Hariharan, P. C.; Pople, J. A. *Mol. Phys.* **1974**, *27*, 209.
(32) Hay, P. J.; Wadt, W. R. *J. Chem. Phys.* **1985**, *82*, 270.
(33) Hay, P. J.; Wadt, W. R. *J. Chem. Phys.* **1985**, *82*, 299.
(34) Wadt, W. R.; Hay, P. J. *J. Chem. Phys.* **1985**, *82*, 284.
(35) Andzelm, J.; Kolmel, C.; Klamt, A. *J. Chem. Phys.* **1995**, *103*, 9312.
(36) Houjou, H.; Inoue, Y.; Sakurai, M. *J. Am. Chem. Soc.* **1998**, *120*, 4459.
(37) Klamt, A.; Schuurmann, G. *J. Chem. Soc., Perkin Trans. 2* **1993**, 799.
(38) Mineva, T.; Russo, N. *Int. J. Quantum Chem.* **1997**, *61*, 665.
(39) Ito, S.; Murakami, T. N.; Comte, P.; Liska, P.; Grätzel, C.; Nazeeruddin, M. K.; Grätzel, M. *Thin Solid Films* **2008**, *516*, 4613.
(40) Ito, S.; Nazeeruddin, K.; Liska, P.; Comte, P.; Charvet, R.; Pechy, P.; Jirousek, M.; Kay, A.; Zakeeruddin, S. M.; Grätzel, M. *Prog. Photovoltaics.* **2006**, *14*, 589.
(41) O'Regan, B. C.; Bakker, K.; Kroeze, J.; Smit, H.; Sommeling, P.; Durrant, J. R. *J. Phys. Chem. B* **2006**, *110*, 17155.

(42) Clifford, J. N.; Palomares, E.; Nazeeruddin, M. K.; Grätzel, M.; Nelson, J.; Li, X.; Long, N. J.; Durrant, J. R. *J. Am. Chem. Soc.* **2004**, *126*, 5225.
(43) Mee, S. P. H.; Lee, V.; Baldwin, J. E. *Chem.—Eur. J.* **2005**, *11*, 3294.
(44) Barolo, C.; Nazeeruddin, M. K.; Fantacci, S.; Di Censo, D.; Comte, P.; Liska, P.; Viscardi, G.; Quagliotto, P.; De Angelis, F.; Ito, S.; Grätzel, M. *Inorg. Chem.* **2006**, *45*, 4642.
(45) Yu, Q.; Liu, S.; Zhang, M.; Cai, N.; Wang, Y.; Wang, P. *J. Phys. Chem. C* **2009**, *113*, 14559.
(46) Kim, J.-J.; Choi, H.; Paek, S.; Kim, C.; Lim, K.; Ju, M.-J.; Kang, H. S.; Kang, M.-S.; Ko, J. *Inorg. Chem.* **2011**, *50*, 11340.
(47) Planells, M.; Pelleja, L.; Clifford, J. N.; Pastore, M.; De Angelis, F.; Lopez, N.; Marder, S. R.; Palomares, E. *Energy Environ. Sci.* **2011**, *4*, 1820.
(48) Gao, F.; Wang, Y.; Zhang, J.; Shi, D.; Wang, M.; Humphry-Baker, R.; Wang, P.; Zakeeruddin, S. M.; Grätzel, M. *Chem. Commun.* **2008**, 2635.
(49) Wang, Z.-S.; Yamaguchi, T.; Sugihara, H.; Arakawa, H. *Langmuir* **2005**, *21*, 4272.
(50) Chiba, Y.; Islam, A.; Watanabe, Y.; Komiya, R.; Koide, N.; Han, L. *Jpn. J. Appl. Phys.* **2006**, *45*, L638.
(51) Fabregat-Santiago, F.; Bisquert, J.; Garcia-Belmonte, G.; Boschloo, G.; Hagfeldt, A. *Sol. Energy Mater. Sol. Cells* **2005**, *87*, 117.
(52) Nishida, J.-i.; Masuko, T.; Cui, Y.; Hara, K.; Shibuya, H.; Ihara, M.; Hosoyama, T.; Goto, R.; Mori, S.; Yamashita, Y. *J. Phys. Chem. C* **2010**, *114*, 17920.
(53) Marinado, T.; Nonomura, K.; Nissfolk, J.; Karlsson, M. K.; Hagberg, D. P.; Sun, L.; Mori, S.; Hagfeldt, A. *Langmuir* **2010**, *26*, 2592.
(54) Koumura, N.; Wang, Z.-S.; Miyashita, M.; Uemura, Y.; Sekiguchi, H.; Cui, Y.; Mori, A.; Mori, S.; Hara, K. *J. Mater. Chem.* **2009**, *19*, 4829.
(55) Matar, F.; Ghaddar, T. H.; Walley, K.; DosSantos, T.; Durrant, J. R.; O'Regan, B. *J. Mater. Chem.* **2008**, *18*, 4246.
(56) Montanari, I.; Nelson, J.; Durrant, J. R. *J. Phys. Chem. B* **2002**, *106*, 12203.
(57) Reynal, A.; Forneli, A.; Palomares, E. *Energy Environ. Sci.* **2010**, *3*, 805.
(58) Privalov, T.; Boschloo, G.; Hagfeldt, A.; Svensson, P. H.; Kloo, L. *J. Phys. Chem. C* **2009**, *113*, 783.